



# Development of a universal, tunable, miniature fluorescence microscope for use at the point of care

CYNTHIA WONG,<sup>1</sup> MICHAL E. PAWLOWSKI,<sup>1</sup> ALESSANDRA FORCUCCI,<sup>1</sup>  
CATHERINE E. MAJORS,<sup>1</sup> REBECCA RICHARDS-KORTUM,<sup>1,2</sup> AND  
TOMASZ S. TKACZYK<sup>1,2,\*</sup>

<sup>1</sup>Department of Bioengineering, Rice University, 6500 Main Street, Houston, TX 77005, USA

<sup>2</sup>Department of Electrical and Computer Engineering, Rice University, 6100 Main Street, Houston, TX 77005, USA

\*[ttkaczyk@rice.edu](mailto:ttkaczyk@rice.edu)

**Abstract:** Fluorescence microscopy can be a powerful tool for cell-based diagnostic assays; however, imaging can be time consuming and labor intensive to perform. Tunable systems give the ability to electronically focus at user selected depths inside an object volume and may simplify the opto-mechanical design of the imaging system. We present a prototype of a universal, tunable, miniature fluorescence microscope built from poly(methyl methacrylate) singlets that incorporates miniature, electrowetted lenses for electronic focusing. We demonstrate the ability of this system to perform clinically relevant differential white blood cell counts using single use custom cartridges pre-loaded with the fluorescent dye acridine orange.

© 2018 Optical Society of America under the terms of the [OSA Open Access Publishing Agreement](#)

**OCIS codes:** (170.2520) Fluorescence microscopy; (170.3880) Medical and biological imaging; (170.1470) Blood or tissue constituent monitoring.

## References and links

1. World Health Organization, "Diagnostic testing," <http://www.who.int/malaria/areas/diagnosis/en/>. Accessed: 29-Jun-2017.
2. World Health Organization, "TB detection and diagnosis," <http://www.who.int/tb/areas-of-work/laboratory/en/>. Accessed: 29-Jun-2017.
3. Nikon MicroscopyU, "Introduction to Fluorescence Microscopy," <https://www.microscopyu.com/techniques/fluorescence/introduction-to-fluorescence-microscopy>. Accessed: 30-Jan-2017.
4. A. Forcucci, M. E. Pawlowski, Z. Crannell, I. Pavlova, R. Richards-Kortum, and T. S. Tkaczyk, "All-plastic miniature fluorescence microscope for point-of-care readout of bead-based bioassays," *J. Biomed. Opt.* **20**(10), 105010 (2015).
5. A. Forcucci, M. E. Pawlowski, C. Majors, R. Richards-Kortum, and T. S. Tkaczyk, "All-plastic, miniature, digital fluorescence microscope for three part white blood cell differential measurements at the point of care," *Biomed. Opt. Express* **6**(11), 4433–4446 (2015).
6. B. F. Grewe, F. F. Voigt, M. van 't Hoff, and F. Helmchen, "Fast two-layer two-photon imaging of neuronal cell populations using an electrically tunable lens," *Biomed. Opt. Express* **2**(7), 2035–2046 (2011).
7. B. Li, H. Qin, S. Yang, and D. Xing, "*In vivo* fast variable focus photoacoustic microscopy using an electrically tunable lens," *Opt. Express* **22**(17), 20130–20137 (2014).
8. Y. Nakai, M. Ozeki, T. Hiraiwa, R. Tanimoto, A. Funahashi, N. Hiroi, A. Taniguchi, S. Nonaka, V. Boilot, R. Shrestha, J. Clark, N. Tamura, V. M. Draviam, and H. Oku, "High-speed microscopy with an electrically tunable lens to image the dynamics of *in vivo* molecular complexes," *Rev. Sci. Instrum.* **86**(1), 013707 (2015).
9. N. Hasan, A. Banerjee, H. Kim, and C. H. Mastrangelo, "Tunable-focus lens for adaptive eyeglasses," *Opt. Express* **25**(2), 1221–1233 (2017).
10. C. L. Grendol, "Apparatus and method for injection molding lenses." US Patent 450534A. Issued: September 10, 1985.
11. Varioptic documentation, "Arctic 316 Family," (Varioptic, 2015).
12. J. M. Cavagnaro, "Polymer optics: progress in plastic optics follows advances in materials and manufacturing," (*Laser Focus World*, 2011), <http://www.laserfocusworld.com/articles/print/volume-47/issue-9/features/polymer-optics-progress-in-plastic-optics-follows-advances-in-materials-and-manufacturing.html>. Accessed: 16-May-2017.

13. M. Kyrish, U. Utzinger, M. R. Descour, B. K. Baggett, and T. S. Tkaczyk, "Ultra-slim plastic endomicroscope objective for non-linear microscopy," *Opt. Express* **19**(8), 7603–7615 (2011).
14. M. D. Chidley, K. D. Carlson, R. R. Richards-Kortum, and M. R. Descour, "Design, assembly, and optical bench testing of a high-numerical-aperture miniature injection-molded objective for fiber-optic confocal reflectance microscopy," *Appl. Opt.* **45**(11), 2545–2554 (2006).
15. SCHOTT Nexterion, "Coverslips," <http://www.schott.com/nexterion/english/products/coverslips.html> Accessed: 16-May-2017.
16. J. F. Jackson, "Supravital Blood Studies, Using Acridine Orange Fluorescence," *Blood* **17**, 643–649 (1961).
17. L. R. Adams and L. A. Kametsky, "Machine characterization of human leukocytes by acridine orange fluorescence," *Acta Cytol.* **15**(3), 289–291 (1971).
18. M. Zheng, J. C. Lin, H. Kasdan, and Y. Tai, "Fluorescent labeling, sensing, and differentiation of leukocytes from undiluted whole blood samples," *Sens. Actuators B Chem.* **132**(2), 558–567 (2008).
19. B. Houwen, "The differential cell count," *Lab. Hematol.* **7**, 89–100 (2001).
20. Centers for Disease Control and Prevention, "Antibiotics Aren't Always the Answer," <https://www.cdc.gov/features/getsmart/index.html>. Accessed: 11 July 2017.
21. C. E. Majors, M. E. Pawlowski, T. Tkaczyk, and R. R. Richards-Kortum, "Low-Cost Disposable Cartridge for Performing a White Blood Cell Count and Partial Differential at the Point-of-Care," *Health Innovation Point of Care Conference*, 1–10 (2014).

## 1. Introduction

Diagnostic tests are essential for rapid and effective health management for a wide range of diseases, from parasitic infections like malaria to infectious diseases like tuberculosis [1,2]. Microscopy has proven to be an important diagnostic tool, particularly at the point of care (POC). However, while allowing easy visualization of pathogens, the diagnostic process is time consuming and labor intensive to perform as the pathogens are often manually counted over multiple fields of view (FOV). Furthermore, visual analysis of images requires a high level of training. To combat these issues, fluorescence microscopy was introduced in the late 19th and early 20th century [3]. Switching from morphological analysis of targets to opto-chemical detection enabled identification of targets by use of fluorescent dyes. This in turn allowed construction of low magnification, large FOV systems that could successfully identify and count infectious agents over large areas, thereby providing clinically necessary statistical information about pathogens of interest.

For example, fluorescence microscopes can be used to quantify specific reaction products by capturing them on fluorescent beads or to quantify the number of white blood cells (WBC) within a patient sample; our lab in particular works on microscopy based POC systems. These systems do not require high resolution or contrast; instead, they rely on target counting (for example, beads or cells) and measuring the color and intensity of fluorescence. Because these systems have low numerical apertures (NA) and low magnifications, they can be designed with large FOV, which allows a single image to include a sufficient number of targets necessary for statistical analysis. While previously developed systems had simple opto-mechanical designs, either the focus needed to be manually adjusted between different fluorescent samples [4] or samples had to be placed within a  $\pm 3 \mu\text{m}$  tolerance [5] due to the depth of field of the system as dictated by the object side NA. These challenges were driven by the design limitations of the sample cartridges used, which, while inexpensive, had looser fabrication tolerances as a tradeoff. Additionally, these previously designed systems needed to be chromatically corrected [5] or required manual adjustment to correct the chromatic focus shift for spectrally separated emission bands of the fluorophores [4]. These systems thus involved balancing manufacturing cost, mechanical complexity, and ease of use.

Tunable lenses have been used in many applications to move the focal plane, such as imaging *in vivo* neuronal and microvasculature structures of mouse brains [6–8]. These lenses have even been integrated into regular eyewear to allow patients to regain their full range of sight [9]. With electrically tunable lenses, changing the power (and thus the focus) of the lens is much faster than mechanically moving either the sample or the system. Additionally, eliminating mechanically moving parts allows for simpler opto-mechanics and the potential for automation.

Thus, to address the difficulties with focus adjustment, sample placement tolerances, and chromatic performance requirements, electrowetted lenses were incorporated in an infinity corrected microscope. The tunable lenses accommodate differences in sample thicknesses and ease the sample placement tolerances while keeping the system itself immobile. Additionally, the tunable lenses allow users to focus on a specific wavelength of interest. The use of electrowetted lenses enables a simplification of the optical design; thus, the system can be comprised of singlets instead of achromatic doublets. By carefully selecting the lens materials, the singlets may even be injection molded [10], suggesting the ability for future mass production of the system. As a validation application, we apply the developed prototype to WBC differential counting, as this test may provide rapid, crucial information regarding infection type and condition of a patient.

## 2. Experimental methods and results

### 2.1 Optical design of a miniature tunable infinity-corrected microscope

An optical schematic of the tunable, miniature, infinity-corrected fluorescence microscope is presented in Fig. 1. The first five lenses comprise the tunable objective assembly (19.6 mm in length), which consists of three singlets made out of an optical grade polymer followed by a tunable lens assembly built out of two Arctic 316 (Varioptic, France) electrowetted lenses, indicated by the two red arrows. The last two lenses comprise the fixed focal length tube lens assembly (7.45 mm in length); both the microscope objective and the tube lens were custom designed in Zemax (Radiant Zemax, USA). The objective assembly is separated from the tube lens assembly by a 6.95 mm infinity corrected space, designed to accommodate passive and removable optical components such as filters and beam splitters.

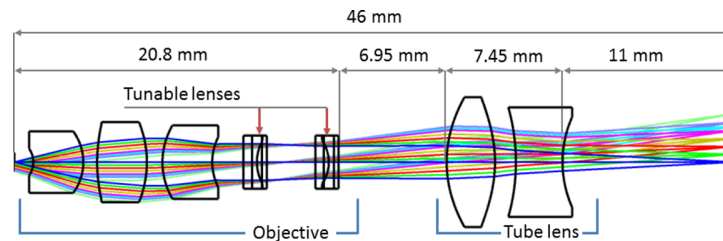


Fig. 1. Optical schematic of the infinity-corrected tunable microscope. The red arrows indicate the tunable Arctic 316 lenses. The first three singlets plus the two tunable lenses comprise the objective while the last two singlets comprise the tube lens. The total length of the system is 46 mm.

Performance of the optical system was optimized for four wavelengths (530, 590, 660 and 720 nm) separated into four monochromatic configurations. Static components were used to minimize wavefront aberrations and the tunable lenses' radii of curvature were used to correct axial chromatic shift between configurations. This approach allowed simplification of the optical design to only three static aspheric lenses in the microscope objective assembly and two fixed lenses in the tube lens assembly. A summary of the optical design parameters of the microscope is presented in Table 1.

Table 1. Summary of optical design parameters of the tunable fluorescence microscope.

Object side Field Of View diameter [mm]	1.2
Objective working distance [mm]	1.2
Object side NA	0.24
Largest Clear Aperture [mm]	8.07
Magnification	-5x
'Infinity space' length [mm]	6.95
Total length of the optical system [mm]	45.0
Curvature of the object surface [mm]	0.0
Curvature of the image surface [mm]	0.0
Telecentricity, object space	Yes

The microscope objective is designed to have an NA of 0.24 and a 1.2 millimeter diameter field of view with largest diameter of the clear aperture slightly below 5 mm. The tube lens' largest clear aperture is 8 mm in diameter, and its working distance is 11 mm. Both the microscope objective and the tube lens form an infinity-corrected microscope with a combined magnification of  $-5\times$ .

The relationship between optical power and voltage for the Arctic 316 is shown in Fig. 2(a). The optical power required to focus the system for each of the four configurations was optimized to be between 35 V and 46 V, which covers a linear and hysteresis free region of power vs. driving voltage curve of the Arctic 316 [11].

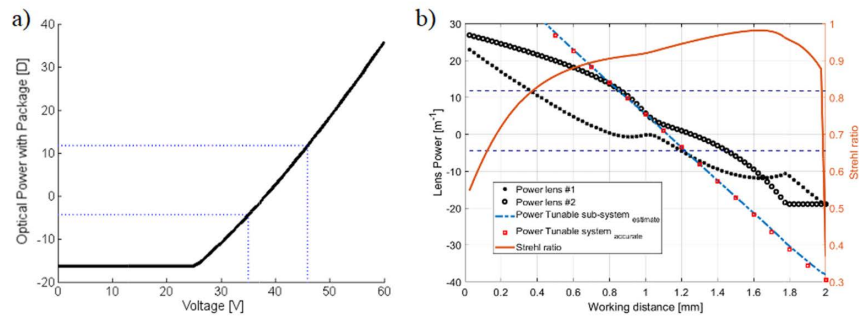


Fig. 2. Typical response of an Arctic 316 tunable lens in response to driving voltage [11] (a). Plot depicting the power of each of the two tunable lenses with respect to the working distance is represented by black dots and circles (b). The dashed blue line shows the estimated power of the electrowetted optics calculated as the sum of the powers of the two tunable lenses. The red squares depict the total power of the tunable sub-system as calculated by a ray tracing algorithm. The Strehl ratio of the system as a function of working distance is plotted with the solid orange line. Calculations were performed at a wavelength of 590 nm. Horizontal dotted lines in both plots depict the linear, hysteresis free region for driving the tunable lenses.

In this region, optical power (OP) of the lens and the driving voltage (DV) can be found using following equation

$$OP = 1.48DV - 56.22 \quad (1)$$

Nominally, at the lowest driving voltage of 35 V the tunable lens has a power of  $-4.52$  D and at 46 V its power increases to  $+11.73$  D [11]. The relationship between lens power and voltage for the tunable lenses at a wavelength of 590 nm can be seen in Fig. 2(b). The horizontal dotted lines represent the linear and hysteresis free region of the power vs. driving voltage as seen in Fig. 2(a). The black dots represent the power of the first tunable lens while the black circles represent the power of the second tunable lens. The blue dashed line is an estimate of the power of the sub-system of the two tunable lenses. The red squares denote the combined power of the two tunable lenses calculated using a ray tracing algorithm. While power of individual lenses changes non-linearly with working distance, due to numerical optimization of performance for each conjugate configuration, the combined power of the tunable sub-assembly changes linearly with working distance. The continuous orange line in Fig. 2(b) depicts the change in the system performance (measured by the Strehl ratio) as a function of working distance. The Strehl ratio changes with working distance; the highest value of 0.98 was for a working distance of 1.62 mm. For the maximum working distance of 2 mm, the Strehl ratio reaches a value of 0.37 and for a working distance of zero (contact imaging), the Strehl ratio was 0.55. Incorporating two tunable lenses allowed for a larger defocus range and a greater control over the focus changes in the tunable system. The optical prescription data of the microscope objective and the tube lens are given in Table 2.

**Table 2. Optical prescription data of the tunable microscope for configurations 1-4\* (Radii, thickness, semi-diameters (SD), and conic values are given in units of [mm])**

Surface	Radii	Thickness	Glass	SD	Conic
0	$\infty$	1.200		0.600	0.000
1	-1.363	3.213	PMMA	0.830	-0.327
2	-3.138	0.892		1.919	-0.037
3	9.850	3.200	PMMA	2.324	-1.761
4	-6.018	1.001		2.488	-1.606
5	4.277	3.202	PMMA	2.288	-0.377
6	3.277	2.003		1.559	-0.361
7	$\infty$	0.550	D263T	1.650	0.000
8	$\infty$	0.320	PC200B**	1.650	0.000
9*	2.988	0.330	H100***, configuration 1	1.350	0.000
	2.789	0.330	H100***, configuration 2		
	2.671	0.330	H100***, configuration 3		
	2.617	0.330	H100***, configuration 4		
10	$\infty$	0.300	D263T	1.350	0.000
11	$\infty$	3.126		1.216	0.000
12	$\infty$	0.550	D263T	1.650	0.000
13	$\infty$	0.320	PC200B**	1.650	0.000
14*	-2.306	0.330	H100***, configuration 1	1.350	0.000
	-2.283	0.330	H100***, configuration 2		
	-2.290	0.330	H100***, configuration 3		
	-2.311	0.330	H100***, configuration 4		
15	$\infty$	0.300	D263T	1.350	0.000
16	$\infty$	6.952		1.350	0.000
17	7.227	3.108	PMMA	4.035	-0.796
18	-7.878	1.345		3.962	-3.772
19	-12.137	3.000	PMMA	3.403	0.000
20	6.674	11.000		2.793	0.000

\*Design optimized for: 530 nm (configuration 1), 590 nm (configuration 2), 660 nm (configuration 3), and 720 nm (configuration 4)

\*\*PC200B data was calculated using the Sellmeier 1 formula with the following coefficients:  $K_1 = 0.909633282$ ,  $L_1 = 0.00633098952$ ,  $K_2 = 0.0326300543$ ,  $L_2 = 0.0516512071$ ,  $K_3 = 2.86366916 \times 10^3$ ,  $L_3 = 1.91154969 \times 10^5$

\*\*\*H100 data was calculated using the Sellmeier 1 formula with the following coefficients:  $K_1 = 0.796282152$ ,  $L_1 = 2.11943907 \times 10^{-7}$ ,  $K_2 = 0.379197157$ ,  $L_2 = 0.0373918648$ ,  $K_3 = 0.118053517$ , and  $L_3 =$

10.4367072 Sellmeier 1 formula used: 
$$n^2 - 1 = \frac{K_1 \lambda^2}{\lambda^2 - L_1} + \frac{K_2 \lambda^2}{\lambda^2 - L_2} + \frac{K_3 \lambda^2}{\lambda^2 - L_3}$$

The selection of materials was driven by the in-house manufacturing process (diamond turning) and the quality of the resultant optics. There are generally three optical polymers that can be single point diamond turned: poly(methyl methacrylate) (PMMA), polystyrene, and cyclo-olefin polymers (COP). To lower cost and simplify manufacturing, it was decided that the entire optical system (excluding the tunable lenses) would be made from PMMA due to its proven machinability on diamond turning lathes [12] and its low autofluorescence [13].



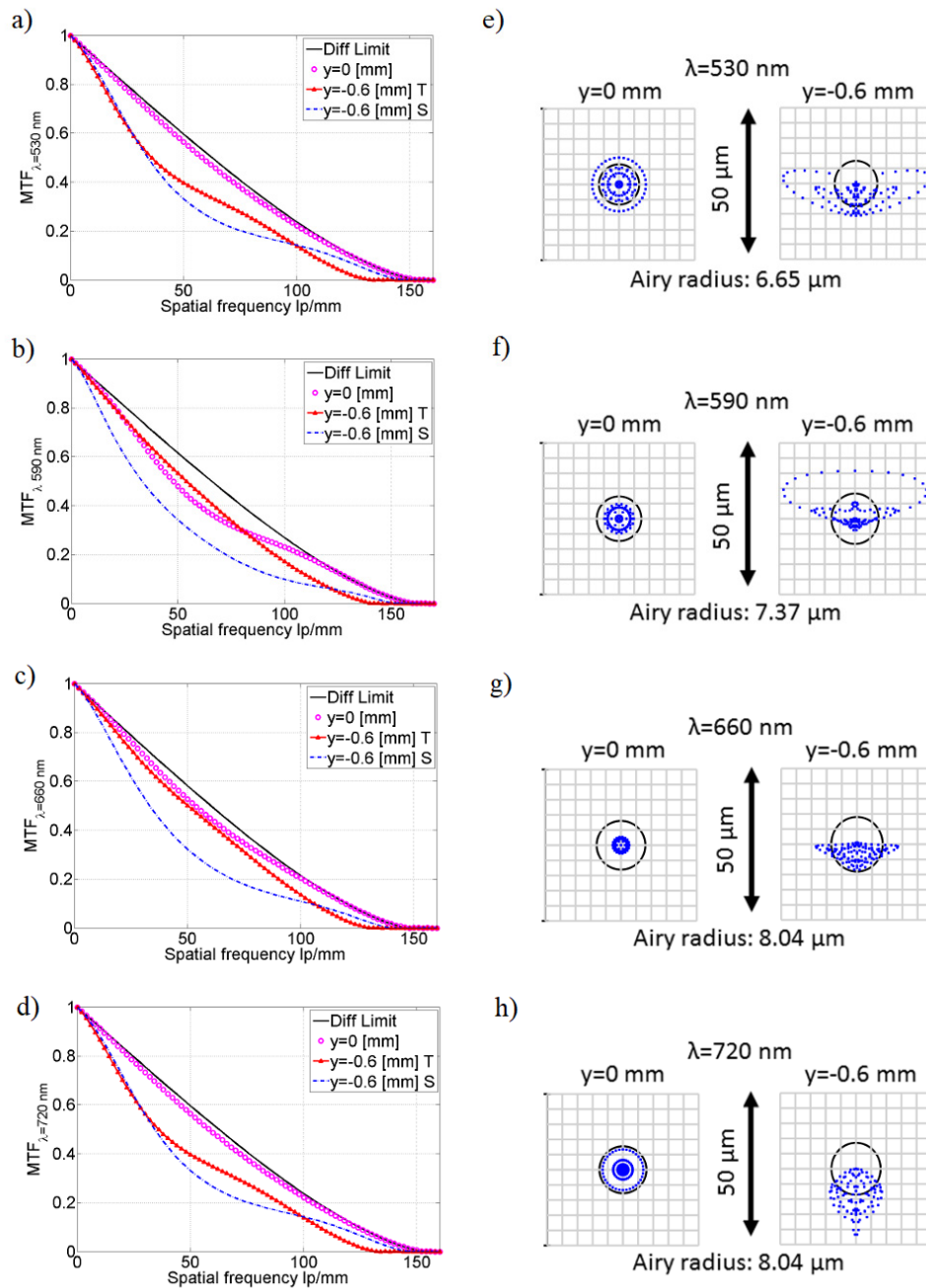


Fig. 3. Performance metrics of the miniature tunable fluorescence microscope for nominal working conditions, calculated for the image plane in both the tangential (T) and sagittal (S) directions. The MTF is shown for (a) 530 nm, (b) 590 nm, (c) 660 nm, and (d) 720 nm configurations. Spots diagrams for the 0.0 mm and 0.60 mm  $y$ -field points are presented in (e-h) for all monochromatic configurations. The Airy disk radii for consecutive configurations is: 6.65  $\mu\text{m}$  for 530 nm, 7.37  $\mu\text{m}$  for 590 nm, 8.04  $\mu\text{m}$  for 660 nm and 8.04  $\mu\text{m}$  for 720 nm.

The design was optimized for eight  $y$ -field points due to the extensive use of aspheric components. The  $y$ -field points used were as follows: 0, 0.1, 0.2, 0.3, 0.4, 0.45, 0.5 and 0.6 mm. The modulation transfer function (MTF) and the spot diagram plots for all

monochromatic configurations for two arbitrary selected object points are presented in Fig. 3. In order to present clear and readable plots, axial and edge field points were selected. Please note that MTF plots for all four wavelengths indicate near diffraction limited performance.

Final system optimization was performed with tolerance operands inserted into the merit function. Tolerances were used to decrease the sensitivity of the design to the manufacturing limitations of the in-house diamond turning process. Surface roughness was not simulated during tolerance analysis, since previously fabricated lenses have been routinely manufactured with an arithmetical mean roughness (Ra) on the order of 10 nm (which is comparable to injection molded optics). Roughness related phenomena like scattering were not considered significant in this project. System performance during optimization was evaluated using the Root Mean Square (RMS) wavefront error. The tolerance values used during this process are presented in Table 3 and were chosen based on empirical evaluation of the in-house manufacturing process. These parameters had been successfully used in previous designs to manufacture customized optical systems [4,5]. The optimized system had a nominal RMS wavefront error of 0.06; the estimated change in performance due to manufacturing tolerances calculated using the Root Sum Square (RSS) algorithm was 0.06 and the total system performance (nominal + change) was assessed to be 0.118.

**Table 3. Tolerance parameters of the miniature tunable microscope**

Parameter	Radii [%]	Thickness [mm]	Element Decenter [mm]	Element Tilt [mm]	Surface Decenter Tilt [mm]	Irregularity [Fringes]	Abbe n
Value	± 0.4%	± 0.02 ± 0.2*	± 0.02	± 0.02	± 0.02	± 0.2	± 2 ± 0.002

Legend for table superscript \*> for surface 17 ('infinity space')

Based on 1000 runs of Monte-Carlo simulations using the RMS spot radius as the criterion, it was estimated that the miniature fluorescence microscope would achieve diffraction limited performance on-axis with an 80% probability. Along the y axis at points 0.1 mm, 0.2 mm, and 0.3 mm, the system had an 80% probability of achieving diffraction limited performance. At field points 0.4 mm and 0.5 mm the system had a 50% chance of achieving diffraction limited performance, and at 0.6 mm field point the system had a 20% chance of achieving diffraction limited performance. Since the system is expected to work with fluorescence samples and does not need to resolve morphological details within the sample of interest, a small drop-off of the contrast due to an increased wavefront error will not have critical influence on the overall performance. Though the residual aberrations could be corrected by additional optical components and/or by tightening manufacturing tolerances, this was avoided in order to produce a cost-balanced system with acceptable performance and satisfactory manufacturing yield.

## 2.2 Mechanical design of the objective

The microscope objective and tube lens were manufactured on a Precitech Optimum 2400 (Ametek, Precitech, Keene, NH, USA), the in-house diamond turning lathe. Pellets of PMMA were mounted on the machine using ER16-UP (Rego-Fix, Tenniken, Switzerland) collets housed in a custom vacuum chuck compatible holder. Diamond turning programs for all surfaces were generated using the Diamond Turning Path Generator program (DTPG v 2.54, Precitech, NH, USA). Contact islands were diamond turned into the lenses in order to provide interfaces with custom brass spacers. The optically non-active external surfaces of all plastic lenses were diamond turned to ensure a transitional fit with the inner diameter of brass tubes, which were used to separately mount static components of the tube lens and the microscope objective.

A cross section of the model of the 3D printed microscope objective holder is displayed in Fig. 4. It contains the three custom PMMA diamond-turned lenses separated by brass spacers. The custom lenses and brass spacers are enclosed in a diamond turned brass tube. The tube is press fit against the two Arctic 316 lenses. The objective holder has a front cap that blocks stray light from entering the optical system and the back end of the threaded holder has an opening for the Arctic 316 wires.

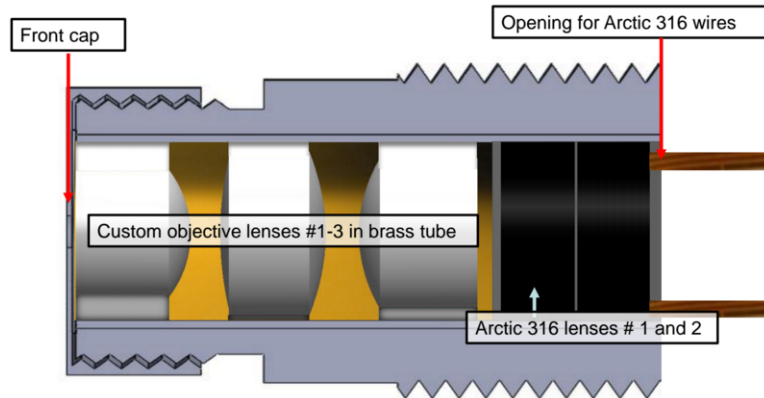


Fig. 4. A cross sectional view of the threaded objective holder, which contains three PMMA singlet aspheric lenses and two Arctic316 electrowetted lenses.

A picture of a tunable Arctic 316 lens is shown in Fig. 5(a). The Arctic 316-P-A model has a straight FlexCable and comes pre-packaged by Varioptic. It has an external diameter of 9.4 mm and a thickness of 3.5 mm. An enclosure was 3D printed to hold the custom objective shown in Fig. 5(b) as well as the two Arctic lenses. Figure 5(b) also presents the assembled static part of the objective in brass tubing (bottom center). Figure 5(c) shows the 3D printed holder for the tube lens.

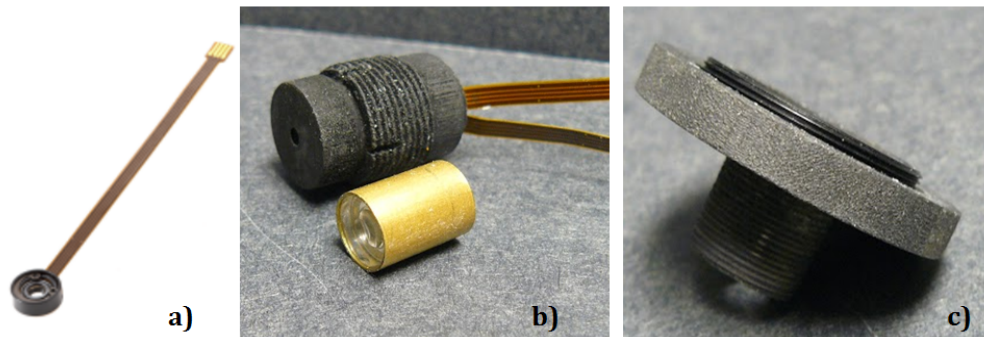


Fig. 5. Components of the miniature tunable microscope: Arctic 316-P tunable lens [11] (a), the 3D printed holder for the tunable objective (b), and the 3D printed tube lens holder with C mount threading for a Flea3 image detector (c).

### 2.3 Tunable objective evaluation

Initial simulations were performed to test the expected chromatic shift of the tunable system. Figure 6 shows the nominal axial chromatic shift in the image space as a function of wavelength for which the system was focused. The wavelengths 450, 550, 600, 650 and 700 nm were chosen to test the monochromatic performance of the tunable objective in a visible part of the electromagnetic spectrum. The location of the plane of best focus is at  $\Delta z$  equal zero.



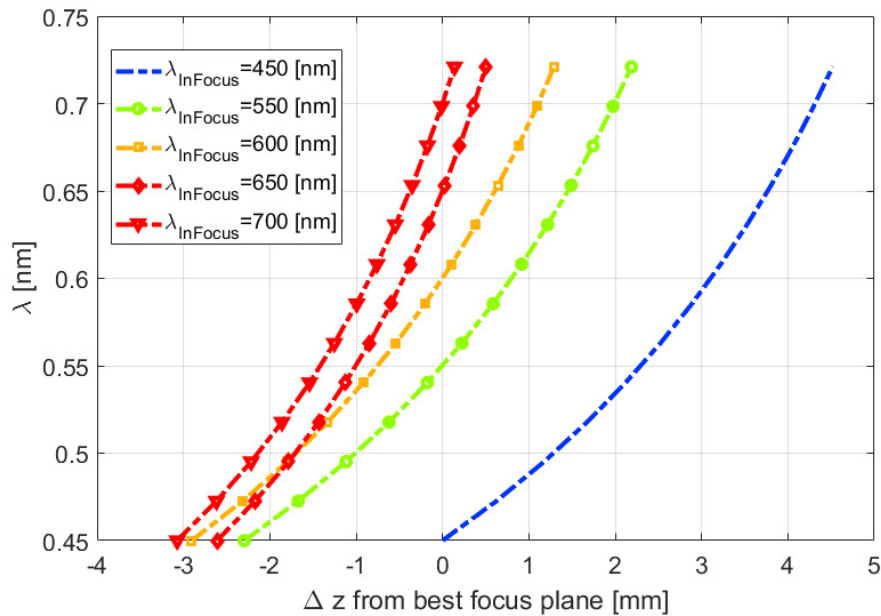


Fig. 6. Plot of the nominal axial chromatic shift in the image space as a function of the focused wavelength. The location of the plane of best focus is when  $\Delta z$  equals zero.

Performance of the system was tested using a positive high resolution 1951 United States Air Force (USAF) target (Stock No. 58-198, Edmund Optics, USA). A white light LED (Part No. MBB1L3, ThorLabs, USA) was coupled to a Köhler illumination system that irradiated the resolution target in trans-illumination to simplify integration and testing, though in the future the tunable microscope will be equipped with an epi-illumination module. During experiments, narrow band interference filters centered at 450, 550, 600, 650 and 700 nm were imaged sequentially. The experiment was performed as follows. First, a 450 nm wavelength excitation filter was placed in the system; the resolution target was brought into focus with the tunable lenses and an image was acquired. Then, the 450 nm filter was sequentially replaced with a 550 nm, 600 nm, 650 nm, and 700 nm filter and an image was acquired at each wavelength respectively, keeping all other system parameters constant. At each wavelength, the best focus was determined qualitatively by the operator. All images were taken with a Point Grey Flea3 color camera (FL3-U3-88S2C-C, Point Grey Inc., Canada) using the manufacturer provided Point Grey FlyCap Software (Point Grey Inc., Canada). Exposure times were 200 ms, 10 ms, 10 ms, 30 ms, and 60 ms for images taken through narrow band filters (from 450 nm to 700 nm respectively) at 0 dB gain. Note that system spatial position was kept constant throughout the experiment; the only components that changed were excitation filters and the tuning of the liquid lenses. The experiment was repeated four additional time, with focus adjustment performed for the next narrow band filter. The final composite collage of 5x5 images is presented in Fig. 7.

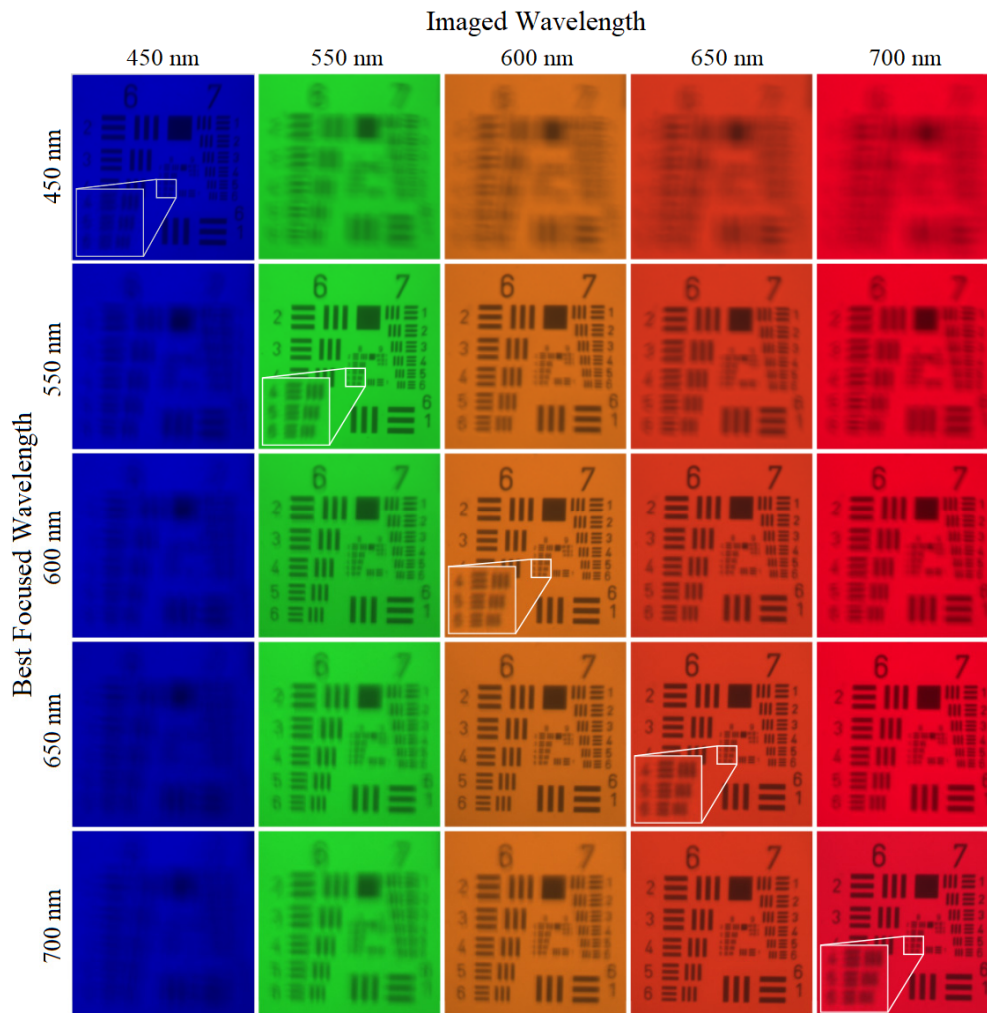


Fig. 7. Images of a positive high resolution USAF target taken with the miniature tunable microscope. The first row represents the system focused at 450 nm, the second row at 550 nm, the third row at 600 nm, the fourth row at 650 nm, and the fifth row at 700 nm. The insets in the bottom left of the main diagonal images are the enlarged Group 8, elements 4-6 of their respective image. Due to the filter and LED combination, the images taken at 450 nm appeared darker than the images at other wavelengths and were contrast enhanced for visualization purposes.

Each row in Fig. 7 shows an image of the USAF target acquired at a fixed driving voltage of the tunable sub-system through all five narrow band filters. Each column depicts the resolution target acquired through a series of five filters at different driving voltages of the tunable lens. Thus, the images on the main diagonal have the maximum contrast for a given combination of focal plane position and narrow band filter. Additionally, the image insets show an enlarged Group 8, elements 4-6 for easier visual assessment of the resolution limits. As one moves vertically through the image matrix presented in Fig. 7, the resolution limit of our system decreases with increased distance from the diagonal. Because we have designed our system to be serially monochromatically corrected, resolution can be recovered by adjusting the driving voltage of the tunable lens, which corresponds to horizontal direction of movement in Fig. 7.

As presented in Fig. 7, the blurring effect is more apparent when the difference in wavelength is 100 nm or larger. For small differences in wavelength (50 nm or less) the blurring can only be seen at very high resolution levels, such as in the areas corresponding to groups 8 and 9 (256.0 to 912.3 line pairs per millimeter). This affects the types of samples that may be imaged.

The theoretically and experimentally verified resolution limit values of the tunable system are summarized in Table 4. The theoretical resolution limit for each wavelength, reported in the second column, was calculated using the Rayleigh criterion

$$d = \frac{0.61\lambda}{NA} \quad (2)$$

Based on the calculated theoretical resolution, the corresponding group and element number on the USAF target was then reported in the third column. The experimental resolution limit was then found by identifying the smallest resolvable element of the USAF target according to the Sparrow resolution limit and was reported in the fourth column. The horizontal intensity cross-sections through the smallest resolvable group of the USAF target, visualized in the fifth column, for the five test wavelengths are presented in the right most column of Table 4. The system was also evaluated using the slanted edge technique [14] yielding a Strehl Ratio of 0.73 (the measurement was performed on-axis for a wavelength of 700 nm). The measured resolution was below nominal for all tested configurations. Based on sensitivity analysis, performance of the tunable system was found to be greatly affected by the alignment of the first lens, followed by tilt and decentration of the second lens (which had half the influence on the RMS wavefront error as compared to the influence of the first lens). Deterioration of performance was likely due to imperfections of the opto-mechanical assembly that relied, in large part, on 3D printed components. Since the system was ultimately designed to work with fluorescently stained samples and was not intended to visualize morphological details at the limit of resolution, the achieved performance was deemed adequate for the application. Note, longer wavelengths showed a drop in resolution compared to shorter wavelengths, as predicted by theory.

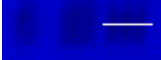
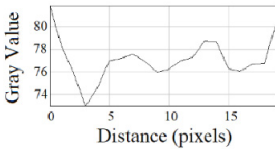

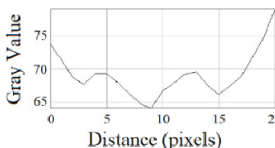

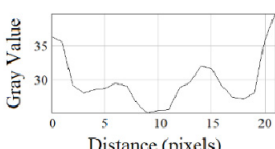

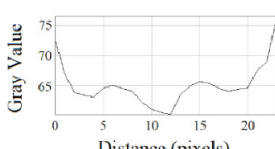

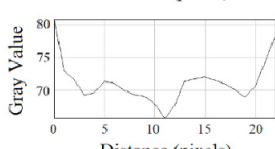
During the design phase, the tunable system was optimized to minimize the change in magnification between all configurations. Magnification of the prototype was experimentally verified to be  $-4.83$ ,  $-4.85$ ,  $-4.76$ ,  $-4.77$ ,  $-4.77$  at the wavelengths 450, 550, 600, 650, and 700 nm respectively. Because measured changes in magnification were on the level of 2%, the system could be considered to have wavelength invariant magnification.

The depth of field (DOF) of a system can be theoretically calculated using the equation

$$d = \frac{\lambda n}{NA^2} \quad (3)$$

Assuming calculations are performed in air ( $n = 1$ ), the shortest DOF of a system with  $NA = 0.24$  will be at a wavelength of 450 nm and will have a value of  $7.8 \mu\text{m}$  while the longest DOF will be at a wavelength of 700 nm and will have a value of  $12.2 \mu\text{m}$ . For the static system previously described [5], the actual precision necessary to place the sample cartridge within the focus plane was within  $\pm 3 \mu\text{m}$ . Manufacturing tolerances (such as coverslip thickness, which range between  $\pm 15\text{-}20 \mu\text{m}$ ) [15] together with the mechanical limitations of the sample loading port make it difficult to obtain focused images for static systems. This issue is typically addressed by adding precision z-stage to microscopes. In order to simplify systems mechanics, tunable lenses may instead be employed to serve this purpose.

**Table 4. Summary of the resolution of the tunable system for 450, 550, 600, 650, and 700 nm wavelengths. The theoretical resolution (located in the ‘Calculated Resolution’ column) was found using the Rayleigh criterion, and the corresponding Group and Element number of the 1951 USAF resolution target is given in the column ‘Resolution Limit (theoretical).’ The experimentally measured resolution was reported in column ‘Resolution Limit (actual).’ The columns ‘Image’ and ‘Intensity Plot’ show the magnified image of the smallest resolvable element of the 1951 USAF target together with the intensity cross-section through the pixels marked with the white line.**

Wavelength	Calculated Resolution (lp/mm)	Resolution Limit (theoretical)	Resolution Limit (actual)	Image	Intensity Plot
450 nm	874.3	Group 9, Element 5	Group 8, Element 6		
550 nm	715.4	Group 9, Element 3	Group 8, Element 6		
600 nm	655.7	Group 9, Element 3	Group 8, Element 5		
650 nm	605.3	Group 9, Element 2	Group 8, Element 4		
700 nm	562.1	Group 9, Element 1	Group 8, Element 4		

To test the defocus range of the system the resolution target was moved as close to the objective as possible and brought into focus using the tunable lenses. A laser-based displacement meter (IL-030, Keyence Corp, Osaka, Japan) was used to measure distance to the resolution target. During the experiment, the resolution target was slowly moved away from the objective while the tunable lenses were used to bring the resolution target into focus. The resolution target was moved until the tunable lenses were unable to bring the Group 7 elements of the target into focus. The total defocus distance of the system was measured to be 830  $\mu\text{m}$ , much larger than the calculated DOF of 7.8-12.2  $\mu\text{m}$ . Electronically controlling the working distance of the microscope allowed for loosened mechanical tolerances of the sample cartridge and contributed to improved user experience.

#### 2.4 Imaging of whole blood samples

In order to demonstrate clinical applicability, the tunable microscope was used to image whole blood stained with acridine orange (AO). WBCs may be fluorescently stained with AO and when excited fluoresce in two spectrally separated bands with emission maxima at 525

and 650 nm when bound to DNA and RNA respectively [16–18]. Based on the ratio between the DNA and RNA signals, WBCs may be divided into three groups: granulocytes, lymphocytes, and monocytes. The ratio of each type of WBC provides a three-part differential count and may be used to distinguish between bacterial and viral infections [19]. This information is important to help determine the most appropriate treatment regimen for the patient, potentially improving therapy outcomes and reducing overuse of antibiotics [20].

To image AO stained whole blood, a 455 nm LED (M455L3, ThorLabs, USA) was used as the illumination source in a trans-illumination configuration along with an excitation filter centered at a wavelength of 470nm (FF01-470/28-25, Semrock, USA). A 532 nm long pass emission filter (BLP01-532R-25, Semrock, USA) was placed between the tube lens and the camera to remove the unwanted background signal. All images were taken using a Point Grey Flea3 color camera (850 ms exposure time, 24 dB gain). Capillary blood from healthy adult donors was used in all experiments and was stained using custom disposable cartridges [21]. The blood was immediately imaged after the samples were prepared. An example image of AO-stained blood taken with the tunable system is presented in Fig. 8.

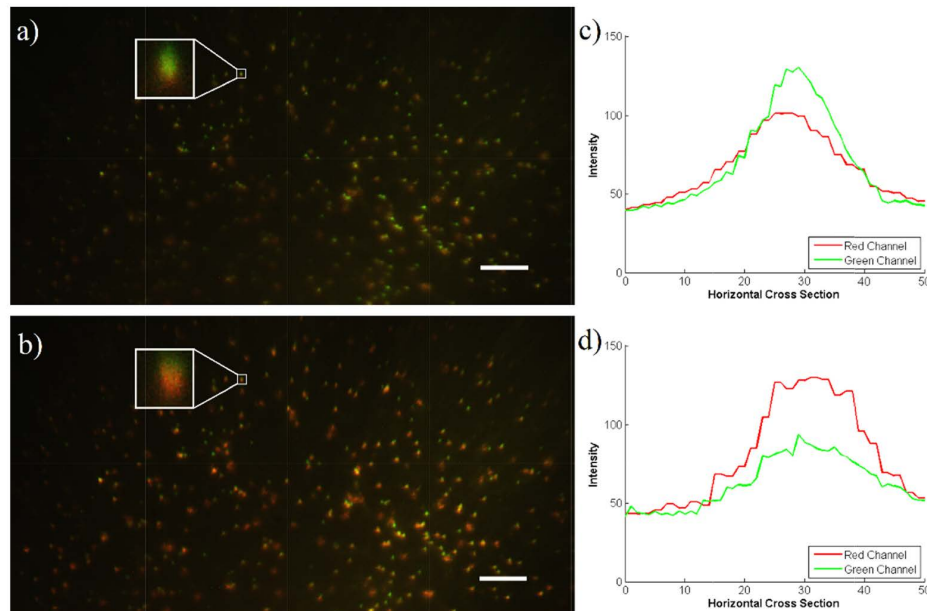


Fig. 8. Example images of AO-stained blood. Image (a) is the sample with the tunable lenses tuned to emphasize the DNA fluorescence in green. Image (b) is the same field of view with the tunable lenses tuned to emphasize the RNA fluorescence in red. The insets of (a) and (b) show a representative WBC. An intensity plot of a horizontal cross section through the center of the WBC shown in (a) and (b) is given in (c) and (d) respectively. Scale bars represent 100  $\mu\text{m}$ . Images have been contrast enhanced for visualization purposes.

First, the system was tuned to bring the DNA fluorescence (at 525 nm) into focus and five consecutive images were taken. Then, the system was tuned to bring the RNA fluorescence (at 650 nm) into focus and a second set of five images were taken. To reduce random noise both sets of five images were averaged (Fig. 8(a) and Fig. 8(b) respectively). The plots in Fig. 8(c) and Fig. 8(d) represent the green and red channel image intensities in a horizontal cross section of a representative WBC (inset images of Fig. 8(a) and Fig. 8(b)). When the system is tuned to bring DNA fluorescence into focus, the green intensity is stronger than the red intensity. Likewise, when the system is tuned to bring RNA fluorescence into focus, the red intensity is stronger than the green intensity. Thus by changing the defocus of the system,



different wavelengths may be emphasized within an image without mechanically moving any part of the system.

The percentages of lymphocytes, monocytes, and granulocytes as well as total WBC counts was calculated using the method described previously [21]. The WBC percentages and counts were taken from the average values of three FOVs from the same sample cartridge. These values were compared to results from a commercial AcT Diff2 hematology analyzer (Beckman Coulter, USA). The results from both systems are shown in Table 5. While the total WBC counts were overestimated using the tunable microscope, the percentages of each sub-type are comparable between the two systems.

**Table 5. Comparison of differential WBC counts from the commercial hematology analyser and the tunable microscope.**

Measurement	Hematology Analyzer	Tunable Microscope
WBC ( $\text{ml}^{-1}$ )	4.80	6.30
Lymphocyte (%)	46.8	41.3
Monocyte (%)	7.7	10.8
Granulocyte (%)	45.5	47.9

In addition to the ability to tune for different wavelengths, the tunable lenses allow the system to image WBCs at different depths in the sample. The inset images in Fig. 9(a) and in Fig. 9(d) show two neighboring WBCs recorded at different depths within the same field of view. When the bottom left WBC transitions from a green intensity to red intensity (as shown in the plots in Fig. 9(b) and Fig. 9(e)), the top right WBC comes into focus (as shown in the intensity plots in Fig. 9(c) and Fig. 9(f)). The sample cartridge blood chamber has a depth of  $88\ \mu\text{m}$  [21], a distance that is much larger than the DOF of  $7.8\text{-}12.2\ \mu\text{m}$ . Because of this, a portion of the WBCs located within the FOV may fall outside the best plane of focus in static imaging systems. While most static systems would thus need to mechanically move either the sample stage or optical system, the incorporated tunable lenses give the ability to electronically change the working distance. With future automation, this may be used to rapidly identify WBCs located in the depth of the sample cartridge within a particular FOV. This is especially important for monocytes that may make up less than one percent of blood volume [19]. Thus, depth tuning may allow for more WBCs to be imaged in the same FOV without the need for lateral scanning and potentially lead to more clinically relevant WBC counts.

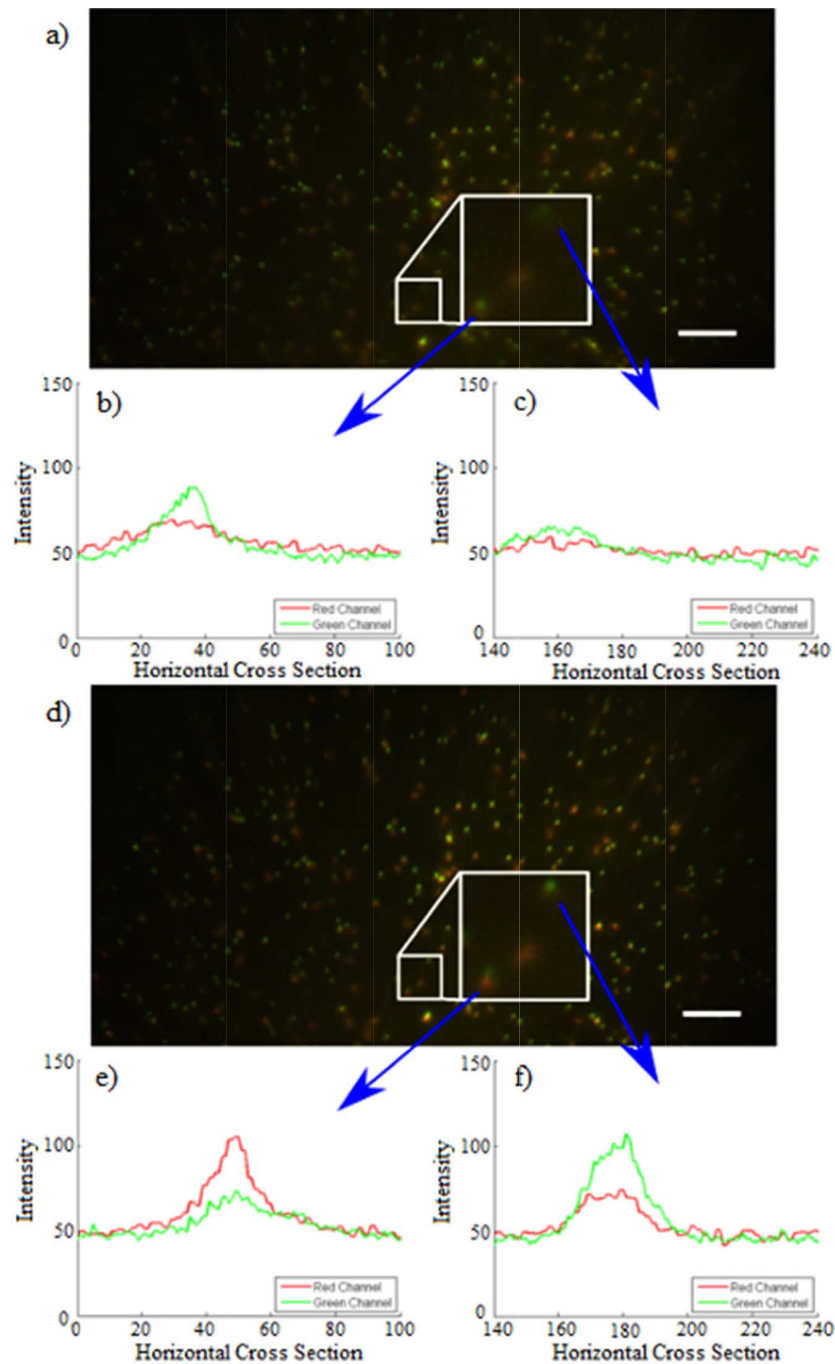


Fig. 9. Imaging WBCs at different depths in AO stained blood. Image (a) is the sample with the tunable lenses tuned to emphasize the DNA fluorescence in green, while (d) is the sample with the tunable lenses tuned to emphasize the RNA fluorescence in red. The intensity plots in (b) and (e) correspond to the bottom left WBC, while the intensity plots in (c) and (f) correspond to the top right WBC. The arrows indicate the WBCs and their corresponding plots. Scale bar represents 100  $\mu\text{m}$ . Images have been contrast enhanced for visualization purposes.

### 3. Conclusions and future work

We designed and fabricated a prototype universal, tunable, miniature fluorescence microscope which can operate in the 525-720 nm spectral range. Our system is characterized by a simple opto-mechanical design with all static singlet lenses made exclusively from PMMA. The singlet design of the optical system allows for easier manufacturing and assembly of the custom fabricated components compared to traditional color corrected systems that use doublets. Additionally, for an optical design comprised solely of singlets, typically unwanted axial chromatic shift is used in our system to spectrally separate fluorophores, which we image sequentially. Lateral chromatic aberration was not accounted for during the optimization stage as it can be corrected for numerically.

The presented system incorporates two miniature electrowetted lenses, to which power of the two lenses can be electronically controlled. This gives us the ability to scan the sample in the axial direction without the need for mechanical components such as stages, and allows us to extend the sample depth range beyond the limit set by theory for static lenses (determined by their depth of field). The two lenses working together allow for a larger defocus range and greater control over the focus changes in the tunable microscope. Electronic focus control gives us ability to extend the system functionality through autofocus and additionally relaxes axial tolerances for sample placement and its geometrical dimensions.

We successfully demonstrated that the system can be used to perform a differential WBC count. However, the tunable miniature fluorescence system may be used to image a variety of sample types/volumes with either single or multiple fluorophores. The infinity-corrected design of the system means that components such as emission filters may be swapped for different applications without requiring a redesign of the optical system. For future work, autofocus and image processing may be incorporated into the system, transforming the microscope into a fully automated device. This may help to increase imaging throughput and allow the device to be operated by less experienced healthcare workers.

#### Funding

National Institutes of Health (NIH) (R21-EB016832); Doris Duke Charitable Foundation (2013138).

#### Disclosures

Tomasz S. Tkaczyk has financial interests in Attoris LLC.